Materials Today Sustainability 19 (2022) 100177

Contents lists available at ScienceDirect

Materials Today Sustainability

journal homepage: https://www.journals.elsevier.com/materials-today-sustainability

Methanol electrosynthesis from CO_2 reduction reaction in polymer electrolyte reactors – fuel cell type using [6,6′-(2,2′-bipyridine-6,6′-diyl)*bis*(1,3,5-triazine-2,4-diamine)] (dinitrate-O) copper (II) complex

L.M.S. Garcia [a], N.G.P. Filho [a], K. Chair [b], P. Kaur [b], A.S. Ramos [a], P.J. Zambiazi [a, *], R.F.B. De Souza [a], L. Otubo [a], A. Duong [b], A.O. Neto [a]

[a] *Instituto de Pesquisas Energéticas e Nucleares, IPEN/CNEN-SP, Av. Prof. Lineu Prestes, 2242 Cidade Universitária, CEP 05508-000, São Paulo, SP, Brazil*
[b] *Département de Chimie, Biochimie et Physique, and Institut de Recherchesur L'Hydrogène, Université Du Québec a Trois-Rivières, Trois-Rivières, Québéc, G9A5H7, Canada*

ARTICLE INFO

Article history:
Received 25 October 2021
Received in revised form
7 June 2022
Accepted 8 June 2022
Available online 14 June 2022

Keywords:
Carbon dioxide reduction reaction
PER-FC
Copper(II) electrocatalysts
Methanol formation
Fuel cell system

ABSTRACT

Electrocatalytic carbon dioxide reduction reaction has been an attractive way to convert greenhouse gas into valuable chemical fuels based on carbon-neutral energy. Therefore, it serves as an effective approach to combating high concentrations of CO_2 in the atmosphere as well as reducing the use of fossil fuels responsible for emitting carbon dioxide and other greenhouse gases, meeting growing energy demands. In this work, the copper(II) *bis*-triazine bipyridine complex supported on carbon black has been applied as a catalyst in a polymeric electrolytic reactor – fuel cell type for converting CO_2 into methanol. The physical and nanostructure properties of the Cu(II) nanocomposite were previously determined by Fourier transform infrared, Raman spectroscopy, X-ray powder diffraction, and transmission electron microscopy techniques. The electrocatalytic activity of the Cu complex catalyst was monitory by differential mass spectroscopy. The results indicate that the catalyst is not selective for the preferential synthesis of a specific product, but a mixture of products (methanol, formic acid, formaldehyde, carbon monoxide, and methane) was detected. According to our results, 2.5% and 5% Cu complex on carbon black were the ideal amounts for polymeric electrolytic reactor – fuel cell type applications to produce methanol from CO_2 with faradaic efficiency of ~22% for both compositions.

1. Introduction

Reductions in CO_2 emissions under the atmosphere have become a high degree of emergency in recent years due to the uncontrolled use of fossil fuels and contemporary deforestation activities. In order to reduce CO_2 concentrations in the atmosphere, carbon dioxide reduction reaction (CO_2RR) is a key tool to slow down climate change resulting from global warming. Therefore, preserving our environment is the need of the moment, and we are looking for strategies to reverse the critical situation in which we are experiencing. One of them consists of transforming CO_2 via electrocatalysis into value-added products/fuels such as carbon monoxide, hydrogen, formic acid, methanol, ethanol, oxalic acid, methane, and many others [1,2]. This strategy, with the reduction of the amount of CO_2, provides possible fuel substitutes for a renewable and clean energy path. However, CO_2 reduction is not a trivial reaction; the linear molecule CO_2 presents two equivalent C=O bonds with binding energy equal to 750 kJ/mol, twice the binding energy compared to other compounds at the same time carbon base [3].

Thermodynamically, the first stage of CO_2 reduction requires one electron with an overpotential of −1.9 V under standard conditions, which is significantly greater than that required for breaking the water molecule into H_2 and oxygen (O_2) [4]. To reduce the overpotential, one of the possible methods is to employ efficient catalysts to drive this reaction. So far, a variety of studies have been reported demonstrating the impact of composition, morphology, and functional groups on different catalytic materials [5]. The most widely used electrocatalysts for CO_2RR reported in the literature are based on precious metals such as Au [6,7], Bi [8,9], Ag [10,11], Pt [12], Pd [12,13], and Sn [14].

* Corresponding author.
E-mail address: pzambiazi@gmail.com (P.J. Zambiazi).

https://doi.org/10.1016/j.mtsust.2022.100177
2589-2347/

It is possible to find some reports in the literature that describe the activity of comparatively cheap metallic copper for CO_2RR [15–19]. Numerous products can be formed by electrocatalysis using this metal such as CH_3OH, CH_2O, HCOOH, CH_4, and CO. And, copper can also facilitate the production of compounds with two carbons atoms, for instance, CH_3CH_2OH, CH_2CH_2, and others. With one of the advances in CO_2RR studies, Lima et al. described the mapping of CO_2 reduction reaction products in potential function using an electrolytic polymeric reactor – fuel cell type (PER-FC), with a proton exchange membrane under mild conditions on Cu/C catalyst [20]. This catalytic activity of Cu is mostly due to the moderate adsorption energy of CO_2 on the surface of copper metal, thus easing its migration [21–23].

Many other studies include the use of metal complexes materials as catalysts to drive CO_2RR, Ma et al. [24] studied the use of a covalent triazine framework that confined copper as an electrocatalyst with the premise of increasing the stability of the metal ions and the selectivity of the CO_2RR over the pure metal. The team has shown that many products such as CH_4, CH_3CH_3, CH_3CH_2OH, and CO could be obtained by electrocatalysis. Hinogami applied the copper rubeanate MOF and obtained greater selectivity for formic acid [25]. Due to the size of the micropores, the dispersion of the MOF active sites, and the improved properties in electronic and protonic conduction, the overpotential could decrease to 0.2 V when compared to a pure copper electrocatalyst in an aqueous electrolyte.

These results could be explained by the aromatic character of the ligands that favor the redox conversion process of the metallic center. This effect can be stabilizing the intermediate M^{+1} species thus facilitating the formation of M-CO_2 bond, which is crucial for the reduction reaction [26]. Furthermore, this type of solid material has a high surface area and microporosity that make the reaction more specific [27]. In addition, the aromatic ligands serve as the adsorption and activations sites for CO_2^- hydrogenation [28–30]. As compared to pure metal catalysts, molecular complexes are advantageous since they contain fewer metal atoms.

In the present report, we investigated the CO_2RR using the [6,6'-(2,2′-bipyridine-6,6′-diyl)*bis*(1,3,5-triazine-2,4-diamine)](dinitrate-*O*)copper(II) complex (Cu complex) in a PER-FC. Cu complex is thermally and chemically stable, and insoluble in water thus the electrocatalysis CO_2 reduction can be performed under heterogeneous conditions. In this work, we coated the carbon Vulcan with the transition metal complex and studied the catalytic activity of this material for CO_2RR.

2. Materials and methods

2.1. Synthesis of Cu complex

All reagents and solvents were used as received from commercial suppliers without further purification. The [6,6'-(2,2′-bipyridine-6,6′-diyl)*bis*(1,3,5-triazine-2,4-diamine)](dinitrate-*O*)copper(II) complex was synthesized according to the reported method [31,32]. The Cu complex was physically mixed with carbon black (Vulcan XC 72R) in the proportions 1%, 2.5%, 5%, 10%, and 20% in carbon (mass/mass).

2.2. Physical properties and nanostructures determination

The Cu complex was characterized by Fourier transform infrared (FT-IR), in an Attenuated Total Reflection (ATR) accessory (MIRacle with a ZnSe Crystal Plate Pike®) installed on a Nicolet® 6700 FT-IR spectrometer equipped with a cooled MCT (Mercury-Cadmium-Telluride) detector. The Raman spectroscopy techniques were performed by Horiba Scientific MacroRam equipment with a wavelength set at 785 nm. The nanostructure was confirmed by the X-ray powder diffraction (XRD) using a diffractometer model Miniflex II, with Cu kα radiation source of 0.15406 Å, set at 2θ range 2–90°, with 2 min^{-1} scan speed. A JEOL JEM-2100 electron microscope operated at 200 kV was used to determine the morphology and structure of the Cu complex nanoparticles.

2.3. Electrochemical measurements

The electrochemical measurements were performed using a three-electrode cell, Ametek PARSTAT 3000A-DX bi-potentiostat/galvanostat. The working electrode is a glassy carbon disc (area = 0.25 cm^2) with 15 μL aliquots of an ink prepared by 8 mg of catalyst, 750 μL of H_2O, 250 μL of isopropyl alcohol, and 15 μL of 5% Nafion D-520. Ag/AgCl (3.0 mol/L KCl) and Pt were used as the reference electrode and the counter electrode (area = 2 cm^2), respectively.

To perform the PER-FC tests and to obtain the polarization curves, the membrane electrode assembly was made with a Nafion® 117 membrane; Pt/C BASF® catalyst (20% by weight and 1 mg cm^{-2}) was used as the anode in gas diffusion electrodes, and catalysts with different Cu complex ratios served as the cathode (5 mg cm^{-2}). The reactor, a 317 L stainless steel cell with unit-type serpentine distribution, supplied H_2 at a flow rate of 200 mL/min with the aid of a temperature-controlled humidifier bottle at a temperature of 80 °C at the anode, and CO_2 at a flow rate of 10 mL/min at room temperature at the cathode. The reaction products resulting from the cathodic effluent output from the PER-FC were analyzed by online differential mass spectroscopy (DMS), as reported by Ramos et al. [33], with quadrupole mass spectrometer, 100 DA QMS 200 M1, Prisma, Pfeiffer equipped with continuous dynode secondary electron multiplier/Faraday cup detector with sensitivity of 200 A/mbar and two differentials pumped chambers: a primary vacuum chamber pumped with a rotary vane pump (DUO 5, Pfeiffer) and a secondary chamber pumped with a turbomolecular pump backed by a dry diaphragm pump (hi-cube 80, Pfeiffer). It was adapted as an interface on top of the primary vacuum chamber separated by a polytetrafluoroethylene membrane (porous size 200 μm Whatman) in a continuous flow, and anodic reaction products were collected by 300s increments of 100 mV monitored by multiple ion detection. The ionic current results were expressed as chemical fragments (m/z) as a potential function.

The products were analyzed by FT-IR spectroscopy technique, in an ATR accessory (MIRacle with a ZnSe Crystal Plate Pike®) installed on a Nicolet® 6700 FT-IR spectrometer equipped with a cooled MCT detector. Liquid N_2 was used to determine the different species formed during the reactor operation of CO_2 reduction reaction at different potentials. The cathodic reaction products were collected by 300s increments of 100 mV, for Faraday efficiency calculation. To quantify the methanol concentration obtained from the solutions collected in the PER-FC, the method applied by Santos [34] was used, and the spectra data were registered in a Horiba Scientific MacroRam Raman spectroscopy equipment with a wavelength set at 785 nm.

3. Results and discussion

The [6,6'-(2,2′-bipiridina-6,6′-diil)*bis*(1,3,5-triazina-2,4-diamina)](dinitrato-*O*)cobre(II) complex was obtained from the reaction between the pre-ligand 6,6'-(2,2′-Bipiridina-6,6′-diil)*bis*(1,3,5-triazina-2,4-diamina) with the copper (II) metal salt, as described by Duong et al. [32]. The molecular structure of the Cu complex is composed by the coordination of the nitrogen atoms present in the tetradentate ligand forming three adjacent five-membered chelate

rings, ensuring the stability of the complex. The distorted octahedral geometry of the complex present coordination of two nitrate co-ligands in the axial positions completing the coordination sphere of the Cu(II) metallic center, as shown in Fig. 1A. Physical and chemical characterizations of the nanostructure copper complex were performed to determine the nanoparticle structural, morphological, crystallographic, and surface state properties. Fig. 1B shows the FT-IR and Raman spectroscopy analyses that were used to determine the structural properties of the ligand and the copper(II) metal center coordination environment of the compound. From the FT-IR spectrum, it is possible to observe the characteristic bands of the tetradentate ligand of the Cu complex, referring to the *bis*-triazine-bipyridine and nitrate ligands, and it is in good agreement with the literature [35]. The NO_3^- co-ligand result in two strong absorptions in the FT-IR spectra at 801 and 1325 cm^{-1} [36], whereas the amine groups bend in the *bis*-triazine-bipyridine ligand; it's characterized by the absorptions symmetrical and asymmetrical stretches in regions of 3069 and 3193 cm^{-1}, respectively. The coordination of the N and O atoms to the metallic center of Cu(II), on the other hand, can be characterized by the stretch found in low-frequency regions of the spectrum [37,38]. The Raman spectroscopy of the Cu complex can characterize two major peaks corresponding to the central metal atom coordination. The metal-donor M-N stretching mode appears in wavenumber regions about 256 cm^{-1} [39]. The nitrate modes were characterized by two peaks to M-ONO_2^- coordination bond in low-

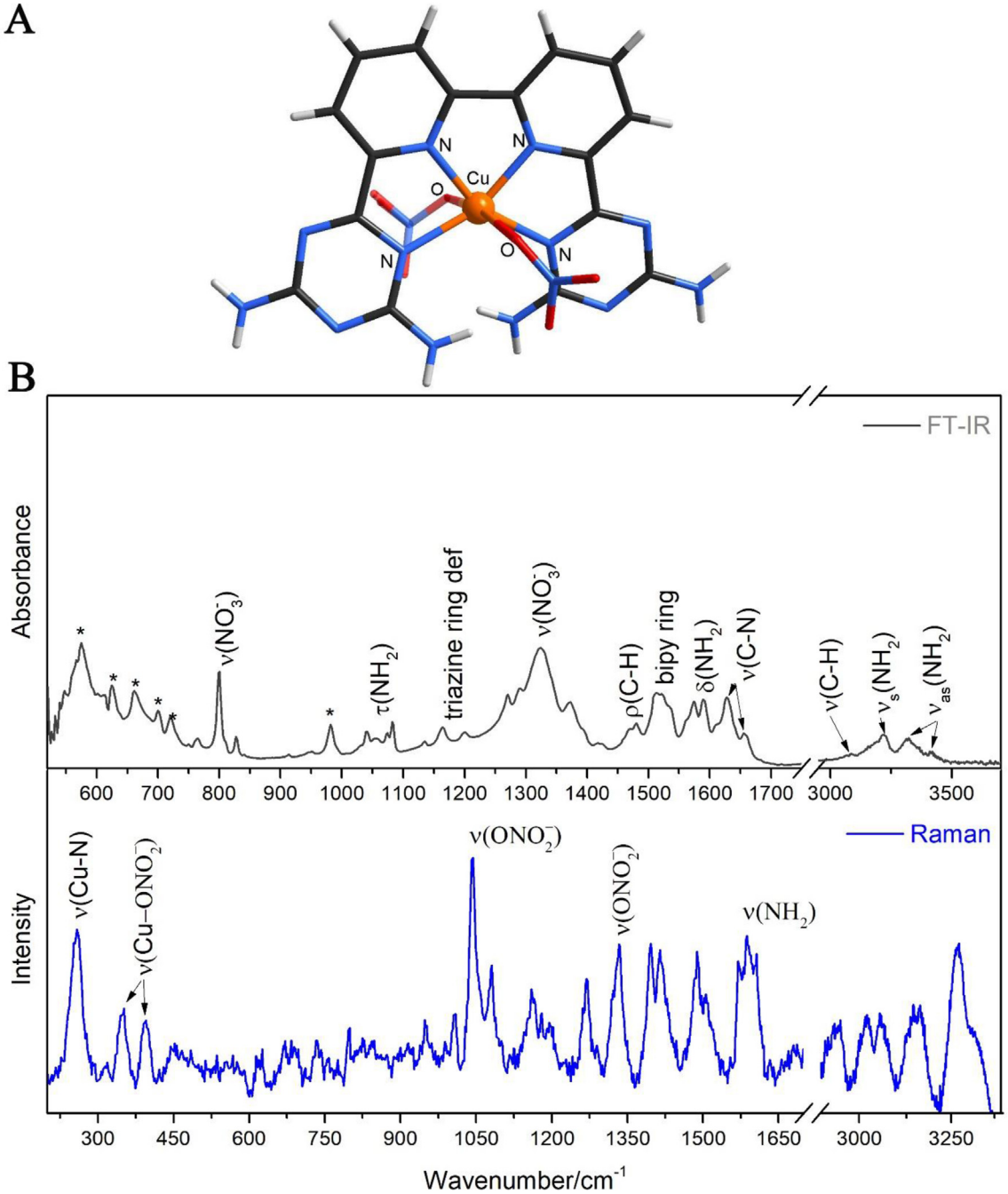

Fig. 1. a) The molecular structure reported by Duong et al. [32]. (b) Structural properties of FT-IR and Raman spectra of the octahedral Cu complex. (*) indicates the band absorption of triazine and bipyridine .

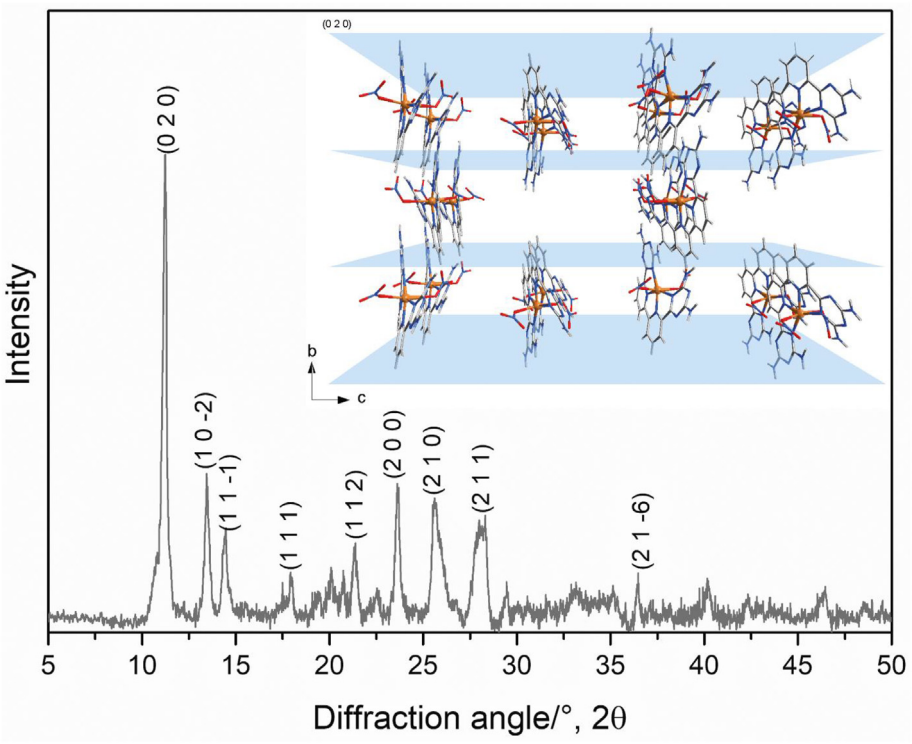

Fig. 2. XRD pattern of the polycrystalline Cu complex and the 3-D crystal structure with highlighted the crystallographic plane (020).

frequency regions at 350 and 395 cm^{-1}, and the stretching mode in high-frequency regions at 1040 and 1332 cm^{-1} [40]. In addition, the peak at 1588 cm^{-1} is a characteristic of the stretching vibration of the amine group, and the other peaks by the heteroaromatic group *bis*-triazine bipyridine ligand [35].

The nanostructure of the Cu complex was analyzed by transmission electron microscopy (TEM) and XRD techniques. Fig. 2 shows the diffraction pattern of the Cu complex and highlights the projection of the crystal structure viewing along the crystallographic axis *a* forming crystal motifs reported by Duong et al. [32].

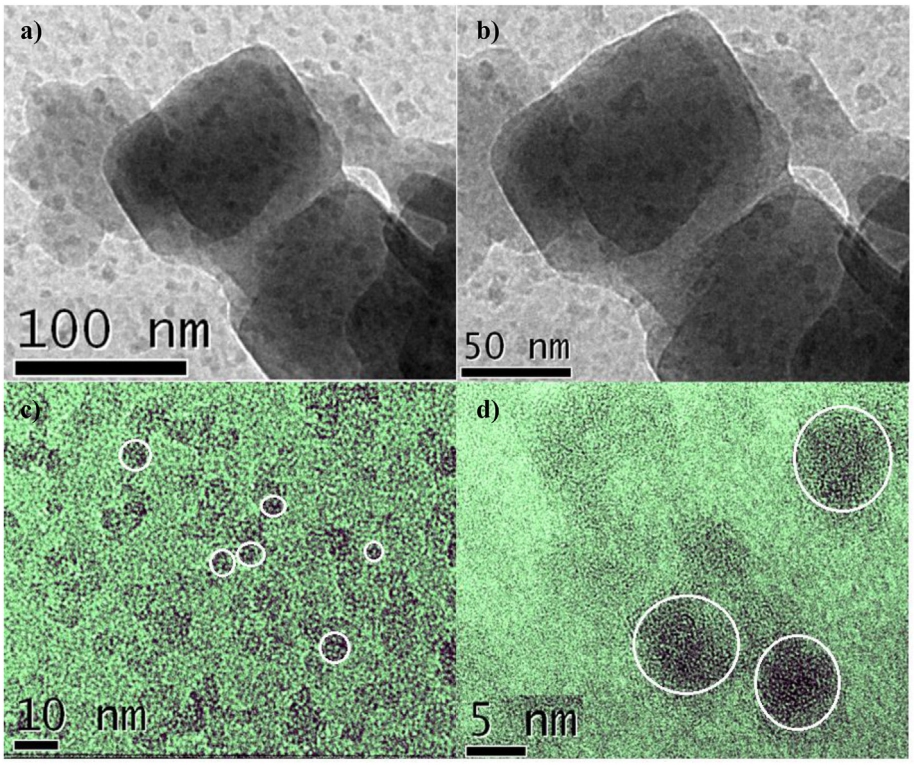

Fig. 3. TEM micrographs of Cu complex nanocrystalline materials at different magnifications: (a) 100 nm and (b) 50 nm with cluster nanoparticles, (c) 10 nm and (d) 5 nm.

The diffraction pattern shows the intense peak at 11.25° corresponds to (0 2 0) plane crystallographic with *d*-spacing equal to 7.89 Å, consistent with observed through the single crystal structure formed by the crystalline packing. In addition, the XRD pattern shows peaks with lower intensity referring to the other crystalline planes. Based on these data, the D_{hkl} crystallites dimension was calculated using the Scherrer equation, and the $D_{(020)}$ value is found as 39.91 nm [41].

The surface morphology and the nanostructure size of the Cu complex were analyzed by TEM, wherein Fig. 3a and b, the formation of irregular regions similar to clusters of Cu complex nanostructure is observed. The TEM micrographs reveal irregular nanocube shape with an average diameter of ~20–40 nm and can be confirmed with the powder XRD experiment discussed previously. A closer examination of the nanocrystalline materials (Fig. 3c and d) allows us to see that the grain boundaries are formed by folds and wrinkles, as characteristic fingerprints. Furthermore, this characterization of the crystal structure can confirm the likely creation of the crystallographic motifs by hydrogen bonds during the polymerization step [42–44]. Besides, from the high-TEM analysis (Fig. 3d), it is possible to see subtly ordered planes that may correspond to the powder diffraction pattern.

For the electrochemical profile analysis of the Cu complex, Fig. 4 shows the cyclic voltammetry of Cu complex/carbon materials with different percentages of the catalyst. It can be noted that with the increasing percentage of Cu complex, two redox peaks appear, one at 0.55 V and another at ~0.37 V, which can be attributed to the oxidation–reduction processes of the copper metal center (II) present in agglomerates or surfaces containing copper [45,46].

The j/V curves for the CO_2 reduction process on PER-FC are shown in Fig. 5a. As can be seen, the amount of Cu complex on carbon increases. These j/V curves were assisted by DMS (Fig. 5) to find out an explanation for this behavior, and as there is more than one possible product for each *m*/*z* ratio, FT-IR measurements were performed with the reactor effluent at different potentials present in S-1. The sample containing only carbon indicated no CO_2 reduction and so it is not included in the current density (I_i) results.

m/z = 46 (Fig. 5a), corresponding to formic acid, was confirmed by a band at 1115 cm^{-1} [47] for all compositions of Cu complex/carbon. The Cu complex 10% presents less negative onset potential than other compositions (~0.3 V). Due to the lower electron energy required for the gas molecule, the formate species, such as formic acid, is the first compound obtained during the CO_2 reduction reaction [48].

The formaldehyde production is observed in I_i for $m/z = 30$ (Fig. 5b) and confirmed by a band at 1249 cm^{-1} corresponding to the CH_2 rock formaldehyde vibration [49] (S-1). It is observed that Cu complex 10% presents a large increment of I_i right after the onset potential (~-0.1 V) and remains more or less stable down to −1.6V, while in the other compositions, this increase occurs more gradually. The curves for I_i for $m/z = 46$ and 28 in which the Cu complex 10% indicates products that require a smaller number of electrons, maybe a justification for the smaller j measured at all potentials.

The Cu complex 20% showed the second-lowest current density, but probably for a different reason than the Cu complex 10% since the products that stand out the most in the DMS and FT-IR measurements are related to methane. The methane production implies more electrons; however, the kinetics occurs slowly. This composition, in addition to presenting the smallest onset for I_i for $m/z = 16$ (−0.45 V), shows the band at an increased wavelength of 1304 cm^{-1} corresponding to (S-1) as compared to the products at −0.4 V and more negative potentials. Cu complex 1% shows the biggest reduction in current density I_i for $m/z = 16$ as compared to other compositions.

For Cu complex 5%, the I_i for $m/z = 28$ attributed to carbon monoxide (~1185 cm^{-1}) showed onset potential near −0.11 V, an increase up to ~ - 0.9V, followed by a decrease. This behavior of increasing I_i for CO production and a succeeding decrease at a certain potential is also observed for Cu complex 2.5%, which shows an onset at ~ −0.2V and a decrease at −0.5 V.

The Cu complex 2.5% also features the largest I_i for methanol ($m/z = 32$) at −1.2V. This alcohol appears at an onset potential of nearly −0.4 V for all materials and displays an increase in I_i with the potential decrease. Methanol is confirmed by $\delta(CH_3)$ bands at 1482 cm^{-1}, 1080 cm^{-1}, and 1030 cm^{-1} (Figure S-1) [34,50] that present similar behavior on intensities as observed by I_i.

In addition to the formation potential of each product, CO_2RR has two important aspects, which would be the rate of the reaction (r) and faradaic efficiency (FE). The reaction rate (r) of methanol production is calculated by Eq. (1) using the methanol quantified by Boyaci's method [51] with the analytical curve constructed in the concentration range of 0.005–1.000 mol/L of methanol. For the following analytical curve, an intensity = 0.9304 + 1.063[methanol] [52] is obtained with the correlation coefficient being 0.932.

$$r = \frac{methanol\ amount}{volume\ x\ time} \tag{1}$$

where r is an important kinetic factor to identify the conversion of CO_2 per unit time and faradaic efficiency. Further FE would be a factor that relates to the amount of energy spent per methanol unit produced and is given by Eq. (2):

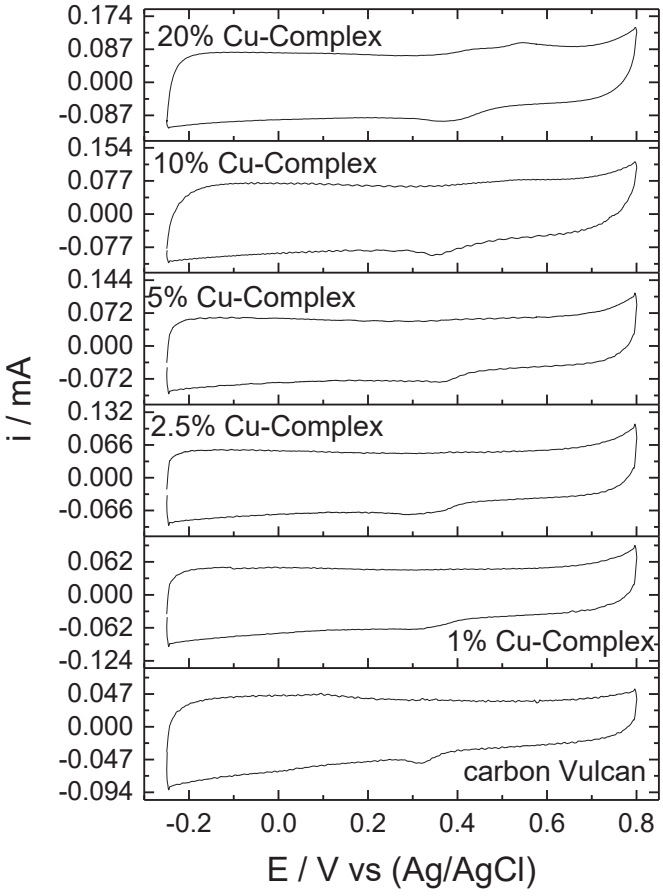

Fig. 4. Cyclic voltammetry of Cu complex/carbon Vulcan material in H_2SO_4 1 mol/L (v = 10 mV/s).

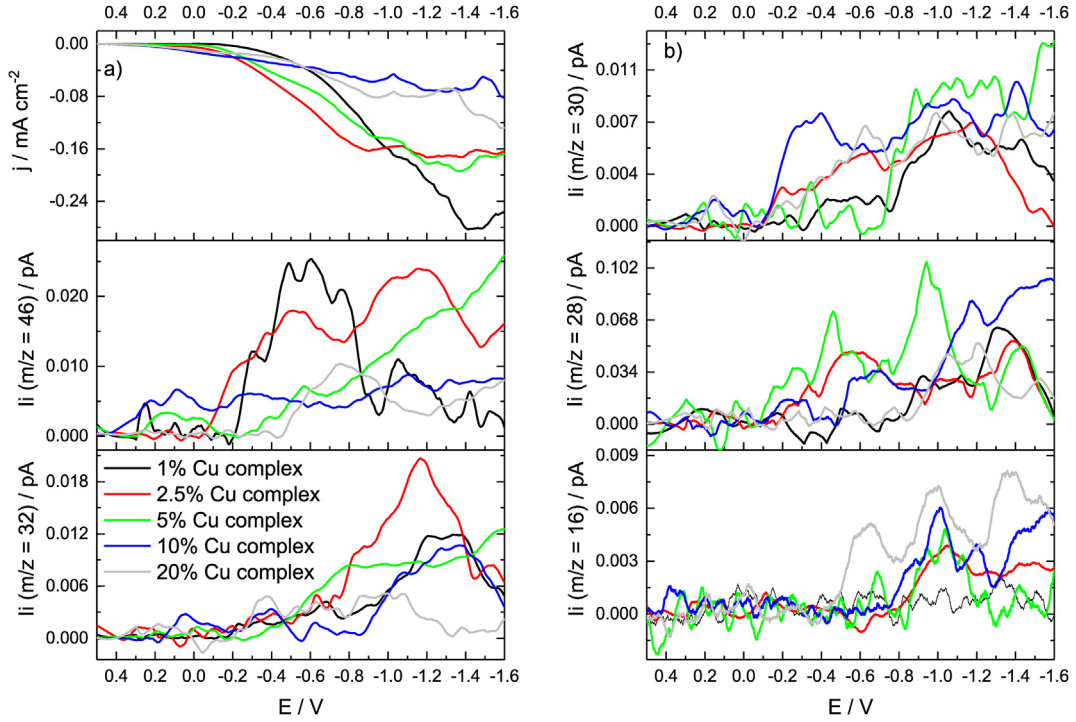

Fig. 5. a) j/V curves, and I_i x potential for *m*/*z* 46 and 32; (b) I_i x potential for *m*/*z* 30, 28, and 16.

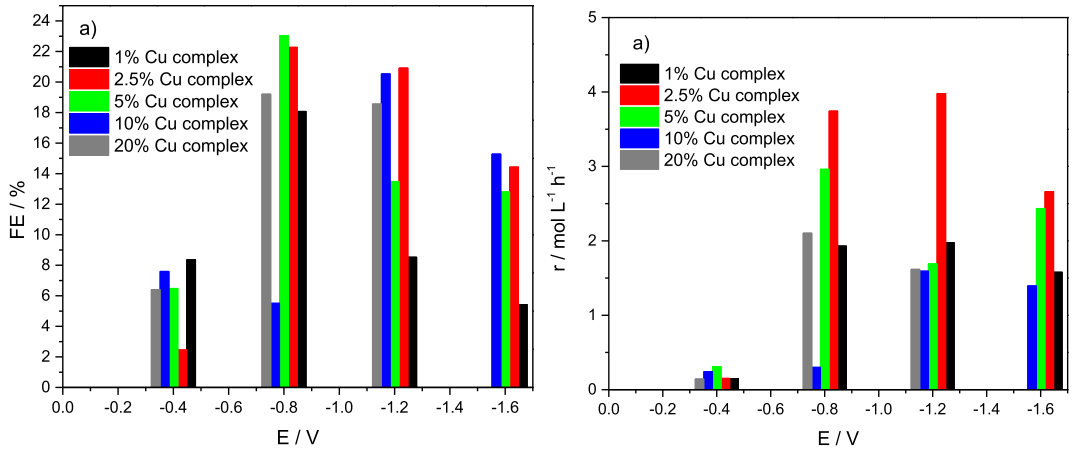

Fig. 6. Methanol efficiency production analysis by (a) Faradaic efficiency (FE), and (b) rate reaction (r) driven under different potentials and proportions of Cu complex catalyst in carbon.

$$FE = \frac{6\ x\ F\ x\ V\ x\ [methanol]}{I\ x\ t} \quad (2)$$

F is the faradaic constant (96487 C/mol), V is the solution volume, [methanol] is the concentration of methanol at the time (t) and I is the current intensity. Fig. 6 summarizes the r and FE under different potentials and proportions of Cu complex in carbon.

In Fig. 6a, for all complex-carbon ratios, they presented similar faradaic efficiencies although there is some difference between these compositions with the potential. However, when looking at the factor (r) Fig. 6b, it is shown that the highest rate reaction is observed for potentials of −0.8 and −1.2V, with Cu complex 2.5% being the most active at all potentials showing the value of r = 3.74 mol L^{-1}/h at −0.8 V and 3.98 mol L^{-1}/h at −1.2 V. Note also that for Cu complex 5%, r is 2.96 mol L^{-1}/h for −0.8 V, which also corresponds to the highest calculated FE of 23% (Fig. 6a). This is followed by Cu complex 2.5%, Cu complex 20%, Cu complex 1%, and Cu complex 10% with FE of 22%, 19.2%, 18%, and 6% respectively.

Electrodes prepared with a low charge of Cu complex, such as 2.5%, were the most active and efficient for the conversion of CO_2 into methanol. This may be due to the formation of agglomerates which decreases the surface energy of the material and, therefore, the catalytic capacity as reported by Garcia [53] for methane partial oxidation with the same Cu complex.

4. Conclusion

The Cu complex can be efficiently used as a catalyst toward CO_2RR electrocatalysis. When added in adequate amounts to carbon, an improvement in the conversion of CO_2 into methanol in a cathode of PER-FC is observed. The DMS results, confirmed by

FT-IR, indicate that the Cu complex catalyst does not determine the selectivity and preferential route for a single product, as different products such as methanol, formic acid, formaldehyde, CO, and methane were detected. However, the relationship between the complex and carbon can shift the starting potentials of these different products to favor a specific product. According to our results, 2.5% and 5% Cu complex were ideal for applications in PER-FC to produce methanol from CO_2. In particular, 2.5% Cu complex could serve as the best candidate since with a faradic efficiency of only 1% less than 5% Cu complex, it showed a 26% higher reaction rate.

Credit author statement

Luis M. S. Garcia: Conceptualization, Validation, Writing – original draft; **Nivaldo G. P. Filho**: Data curation, Validation, Writing – original draft preparation; **Khaoula Chair:** Writing – reviewing and editing; **Prabhjyot Kaur**: Writing – reviewing and editing; **Andrezza S. Ramos**: Validation, Writing and editing; **Priscilla J. Zambiazi**: Data curation, Writing – original draft preparation, Visualization; **Rodrigo F. B. De Souza**: Conceptualization, Data curation, Writing – original draft preparation, Visualization; **Larissa Otubo**: Formal analysis, Validation; **Adam Duong**: Resources, Writing – review and editing, Investigation; **Almir O. Neto**: Supervision, Project administration, Writing – review and editing.

Declaration of competing interest

The authors declare that they have no known competing financial interests or personal relationships that could have appeared to influence the work reported in this article.

Acknowledgments

The authors are grateful to CAPES, CNPq (302709/2020-7), CINE-SHELL (ANP)/FAPESP grants 2017/11937-4, the Natural Sciences and Engineering Research Council of Canada (RGPIN-2015-06425), the Canada Foundation for Innovation, and the Université du Québec à Trois-Rivières for financial supports.

Appendix A. Supplementary data

Supplementary data to this article can be found online at https://doi.org/10.1016/j.mtsust.2022.100177.

References

[1] D. Ješić, D. Lašič Jurković, A. Pohar, L. Suhadolnik, B. Likozar, Engineering photocatalytic and photoelectrocatalytic CO2 reduction reactions: mechanisms, intrinsic kinetics, mass transfer resistances, reactors and multi-scale modelling simulations, Chem. Eng. J. 407 (2021) 126799.
[2] C. Kim, F. Dionigi, V. Beermann, X. Wang, T. Möller, P. Strasser, Alloy nanocatalysts for the electrochemical oxygen reduction (ORR) and the direct electrochemical carbon dioxide reduction reaction (CO2RR), Adv. Mater. 31 (31) (2019) 1805617.
[3] A.A. Khan, M. Tahir, Recent advancements in engineering approach towards design of photo-reactors for selective photocatalytic CO2 reduction to renewable fuels, J. CO2 Util. 29 (2019) 205–239.
[4] H. Ooka, M.C. Figueiredo, M.T.M. Koper, Competition between hydrogen evolution and carbon dioxide reduction on copper electrodes in mildly acidic media, Langmuir 33 (37) (2017) 9307–9313.
[5] C. Bai, L. An, J. Zhang, X. Zhang, B. Zhang, L. Qiang, Y. Yu, J. Zhang, Superlow friction of amorphous diamond-like carbon films in humid ambient enabled by hexagonal boron nitride nanosheet wrapped carbon nanoparticles, Chem. Eng. J. 402 (2020) 126206.
[6] D.R. Kauffman, D.R. Alfonso, D.N. Tafen, C. Wang, Y. Zhou, Y. Yu, J.W. Lekse, X. Deng, V. Espinoza, J. Trindell, O.K. Ranasingha, A. Roy, J.-S. Lee, H.L. Xin, Selective electrocatalytic reduction of CO2 into CO at small, thiol-capped Au/Cu nanoparticles, J. Phys. Chem. C 122 (49) (2018) 27991–28000.
[7] H. Mistry, R. Reske, Z. Zeng, Z.-J. Zhao, J. Greeley, P. Strasser, B.R. Cuenya, Exceptional size-dependent activity enhancement in the electroreduction of CO2 over Au nanoparticles, J. Am. Chem. Soc. 136 (47) (2014) 16473–16476.
[8] A. Atifi, T.P. Keane, J.L. DiMeglio, R.C. Pupillo, D.R. Mullins, D.A. Lutterman, J. Rosenthal, Insights into the composition and function of a bismuth-based catalyst for reduction of CO2 to CO, J. Phys. Chem. C 123 (14) (2019) 9087–9095.
[9] Z. Zhang, M. Chi, G.M. Veith, P. Zhang, D.A. Lutterman, J. Rosenthal, S.H. Overbury, S. Dai, H. Zhu, Rational design of Bi nanoparticles for efficient electrochemical CO2 reduction: the elucidation of size and surface condition effects, ACS Catal. 6 (9) (2016) 6255–6264.
[10] S.Y. Chae, S.Y. Lee, O.-S. Joo, Directly synthesized silver nanoparticles on gas diffusion layers by electrospray pyrolysis for electrochemical CO2 reduction, Electrochim. Acta 303 (2019) 118–124.
[11] C. Kim, T. Eom, M.S. Jee, H. Jung, H. Kim, B.K. Min, Y.J. Hwang, Insight into electrochemical CO2 reduction on surface-molecule-mediated Ag nanoparticles, ACS Catal. 7 (1) (2017) 779–785.
[12] D. Gao, J. Wang, H. Wu, X. Jiang, S. Miao, G. Wang, X. Bao, pH effect on electrocatalytic reduction of CO2 over Pd and Pt nanoparticles, Electrochem. Commun. 55 (2015) 1–5.
[13] D. Gao, H. Zhou, J. Wang, S. Miao, F. Yang, G. Wang, J. Wang, X. Bao, Size-dependent electrocatalytic reduction of CO2 over Pd nanoparticles, J. Am. Chem. Soc. 137 (13) (2015) 4288–4291.
[14] J.T. Feaster, C. Shi, E.R. Cave, T. Hatsukade, D.N. Abram, K.P. Kuhl, C. Hahn, J.K. Nørskov, T.F. Jaramillo, Understanding selectivity for the electrochemical reduction of carbon dioxide to formic acid and carbon monoxide on metal electrodes, ACS Catal. 7 (7) (2017) 4822–4827.
[15] F. Calle-Vallejo, M.T. Koper, Theoretical considerations on the electroreduction of CO to C2 species on Cu(100) electrodes, Angew. Chem., Int. Ed. 52 (28) (2013) 7282–7285.
[16] M.K. Kim, H.J. Kim, H. Lim, Y. Kwon, H.M. Jeong, Metal–organic framework-mediated strategy for enhanced methane production on copper nanoparticles in electrochemical CO2 reduction, Electrochim. Acta 306 (2019) 28–34.
[17] Z. Tao, Z. Wu, X. Yuan, Y. Wu, H. Wang, Copper–gold interactions enhancing formate production from electrochemical CO2 reduction, ACS Catal. 9 (12) (2019) 10894–10898.
[18] Y. Takatsuji, I. Nakata, M. Morimoto, T. Sakakura, R. Yamasaki, T. Haruyama, Highly selective methane production through electrochemical CO2 reduction by electrolytically plated Cu-Co electrode, Electrocatalysis 10 (1) (2019) 29–34.
[19] D. Yang, Q. Zhu, C. Chen, H. Liu, Z. Liu, Z. Zhao, X. Zhang, S. Liu, B. Han, Selective electroreduction of carbon dioxide to methanol on copper selenide nanocatalysts, Nat. Commun. 10 (1) (2019) 677.
[20] M. Lima, C.M. Godoi, M.C.L. Santos, J. Nandenha, A.O. Neto, R.F.B. De Souza, CO2 reduction on Cu/C used as a cathode in a polymeric electrolyte reactor - fuel cell type, Int. J. Hydrog. Energy 47 (6) (2022) 4010–4017.
[21] A. Bagger, W. Ju, A.S. Varela, P. Strasser, J. Rossmeisl, Electrochemical CO(2) reduction: a classification problem, ChemPhysChem 18 (22) (2017) 3266–3273.
[22] A. Wuttig, C. Liu, Q. Peng, M. Yaguchi, C.H. Hendon, K. Motobayashi, S. Ye, M. Osawa, Y. Surendranath, Tracking a common surface-bound intermediate during CO2-to-Fuels catalysis, ACS Cent. Sci. 2 (8) (2016) 522–528.
[23] A. Vasileff, X. Zhi, C. Xu, L. Ge, Y. Jiao, Y. Zheng, S.-Z. Qiao, Selectivity control for electrochemical CO2 reduction by charge redistribution on the surface of copper alloys, ACS Catal. 9 (10) (2019) 9411–9417.
[24] L. Ma, W. Hu, B. Mei, H. Liu, B. Yuan, J. Zang, T. Chen, L. Zou, Z. Zou, B. Yang, Y. Yu, J. Ma, Z. Jiang, K. Wen, H. Yang, Covalent triazine framework confined copper catalysts for selective electrochemical CO2 reduction: operando diagnosis of active sites, ACS Catal. 10 (8) (2020) 4534–4542.
[25] R. Hinogami, S. Yotsuhashi, M. Deguchi, Y. Zenitani, H. Hashiba, Y. Yamada, Electrochemical reduction of carbon dioxide using a copper rubeanate metal organic framework, ECS Electrochem. Lett. 1 (4) (2012) H17–H19.
[26] S. Singh, B. Phukan, C. Mukherjee, A. Verma, Salen ligand complexes as electrocatalysts for direct electrochemical reduction of gaseous carbon dioxide to value added products, RSC Adv. 5 (5) (2015) 3581–3589.
[27] R. Babu, A.C. Kathalikkattil, R. Roshan, J. Tharun, D.-W. Kim, D.-W. Park, Dual-porous metal organic framework for room temperature CO2 fixation via cyclic carbonate synthesis, Green Chem. 18 (1) (2016) 232–242.
[28] C.D. Windle, R.N. Perutz, Advances in molecular photocatalytic and electrocatalytic CO2 reduction, Coord. Chem. Rev. 256 (21) (2012) 2562–2570.
[29] S. Gu, A.N. Marianov, Y. Zhu, Y. Jiang, Cobalt porphyrin immobilized on the TiO2 nanotube electrode for CO2 electroreduction in aqueous solution, J. Energy Chem. 55 (2021) 219–227.
[30] D. Gao, T. Liu, G. Wang, X. Bao, Structure sensitivity in single-atom catalysis toward CO2 electroreduction, ACS Energy Lett. 6 (2) (2021) 713–727.
[31] A. Duong, T. Maris, O. Lebel, J.D. Wuest, Syntheses and structures of isomeric diaminotriazinyl-substituted 2,2′-bipyridines and 1,10-phenanthrolines, J. Org. Chem. 76 (5) (2011) 1333–1341.
[32] S. Rajak, O. Schott, P. Kaur, T. Maris, G.S. Hanan, A. Duong, Mimicking 2,2′:6′,2″:6″,2‴-quaterpyridine complexes for the light-driven hydrogen evolution reaction: synthesis, structural, thermal and physicochemical characterizations, RSC Adv. 9 (48) (2019) 28153–28164.

[33] A.S. Ramos, M.C.L. Santos, C.M. Godoi, A. Oliveira Neto, R.F.B. De Souza, Obtaining C2 and C3 products from methane using Pd/C as anode in a solid fuel cell-type electrolyte reactor, ChemCatChem 12 (18) (2020) 4517–4521.
[34] M.C.L. Santos, L.C. Nunes, L.M.G. Silva, A.S. Ramos, F.C. Fonseca, R.F.B. de Souza, A.O. Neto, Direct alkaline anion exchange membrane fuel cell to converting methane into methanol, ChemistrySelect 4 (39) (2019) 11430–11434.
[35] Applications in inorganic chemistry, in: Infrared and Raman Spectra of Inorganic and Coordination Compounds, 2008, pp. 149–354.
[36] Z. Boutobba, A. Direm, K. Sayin, B. El Bali, M. Lachkar, N. Benali-Cherif, Crystal structure, Hirshfeld surface analysis and theoretical calculations of an oxalato-bridged copper(II) complex: μ-oxalato-bis[(2,2'-bipyridine) hydrate copper(II) nitrate], J. Iran. Chem. Soc. 17 (3) (2020) 671–685.
[37] A. Hussain, M.F. AlAjmi, M.T. Rehman, S. Amir, F.M. Husain, A. Alsalme, M.A. Siddiqui, A.A. AlKhedhairy, R.A. Khan, Copper(II) complexes as potential anticancer and Nonsteroidal anti-inflammatory agents: in vitro and in vivo studies, Sci. Rep. 9 (1) (2019) 5237.
[38] P. Ruíz, R. Ortiz, L. Perelló, G. Alzuet, M. González-Álvarez, M. Liu-González, F. Sanz-Ruíz, Synthesis, structure, and nuclease properties of several binary and ternary complexes of copper(II) with norfloxacin and 1,10 phenantroline, J. Inorg. Biochem. 101 (5) (2007) 831–840.
[39] J. Sharma, Z. Jiang, A. Bhutani, P. Behera, D.P. Shoemaker, A unique copper coordination structure with both mono- and bi-dentate ethylenediamine ligands, CrystEngComm 21 (17) (2019) 2718–2726.
[40] Y. Suffren, F.-G. Rollet, C. Reber, Raman spectroscopy of transition metal complexes: molecular vibrational frequencies, phase transitions, isomers, and electronic structure, Comments Inorg. Chem. 32 (5–6) (2011) 246–276.
[41] U. Holzwarth, N. Gibson, The Scherrer equation versus the 'Debye-Scherrer equation', Nat. Nanotechnol. 6 (9) (2011) 534.
[42] Y. Liu, Y. Zhang, X. Li, X. Gao, X. Niu, W. Wang, Q. Wu, Z. Yuan, Fluorescence-enhanced covalent organic framework nanosystem for tumor imaging and photothermal therapy, Nanoscale 11 (21) (2019) 10429–10438.
[43] N.A. Khan, J. Yuan, H. Wu, T. Huang, X. You, A.U. Rahman, C.S. Azad, M.A. Olson, Z. Jiang, Covalent organic framework nanosheets as reactive fillers to fabricate free-standing polyamide membranes for efficient desalination, ACS Appl. Mater. Interfaces 12 (24) (2020) 27777–27785.
[44] A. Khalajhedayati, Z. Pan, T.J. Rupert, Manipulating the interfacial structure of nanomaterials to achieve a unique combination of strength and ductility, Nat. Commun. 7 (1) (2016) 10802.
[45] C.A. Ottoni, C.E.D. Ramos, R.F.B. de Souza, S.G. da Silva, E.V. Spinace, A.O. Neto, Glycerol and ethanol oxidation in alkaline medium using PtCu/C electrocatalysts, Int. J. Electrochem. Sci. 13 (2) (2018) 1893–1904.
[46] H. Hosseini, H. Ahmar, A. Dehghani, A. Bagheri, A.R. Fakhari, M.M. Amini, Au-SH-SiO2 nanoparticles supported on metal-organic framework (Au-SH-SiO2@Cu-MOF) as a sensor for electrocatalytic oxidation and determination of hydrazine, Electrochim. Acta 88 (2013) 301–309.
[47] B.S. Beckingham, N.A. Lynd, D.J. Miller, Monitoring multicomponent transport using in situ ATR FTIR spectroscopy, J. Membr. Sci. 550 (2018) 348–356.
[48] X. Chen, Z.-Z. Lin, M. Ju, L.-X. Guo, Confined electrochemical catalysis under cover: enhanced CO2 reduction at the interface between graphdiyne and Cu surface, Appl. Surf. Sci. 479 (2019) 685–692.
[49] J. Liu, H.-T. Kim, S.L. Anderson, Multiphoton ionization and photoelectron spectroscopy of formaldehyde via its 3p Rydberg states, J. Chem. Phys. 114 (22) (2001) 9797–9806.
[50] J. Nandenha, R.M. Piasentin, L.M.G. Silva, E.H. Fontes, A.O. Neto, R.F.B. de Souza, Partial oxidation of methane and generation of electricity using a PEMFC, Ionics 25 (10) (2019) 5077–5082.
[51] I.H. Boyaci, H.E. Genis, B. Guven, U. Tamer, N. Alper, A novel method for quantification of ethanol and methanol in distilled alcoholic beverages using Raman spectroscopy, J. Raman Spectrosc. 43 (8) (2012) 1171–1176.
[52] M. Zhiani, S. Majidi, H. Rostami, M.M. Taghiabadi, Comparative study of aliphatic alcohols electrooxidation on zero-valent palladium complex for direct alcohol fuel cells, Int. J. Hydrogen Energy 40 (1) (2015) 568–576.
[53] L.M.S. Garcia, S. Rajak, K. Chair, C.M. Godoy, A.J. Silva, P.V.R. Gomes, E.A. Sanches, A.S. Ramos, R.F.B. De Souza, A. Duong, A.O. Neto, Conversion of methane into methanol using the [6,6'-(2,2'-Bipyridine-6,6'-Diyl)bis(1,3,5-Triazine-2,4-Diamine)](Nitrato-O)copper(II) complex in a solid electrolyte reactor fuel cell type, ACS Omega 5 (26) (2020) 16003–16009.